Self-organized Translational Wheeling Motion in Stochastic Self-Assembling Modules

Shuhei Miyashita[1]*, Kohei Nakajima[2], Zoltán Nagy[3], and Rolf Pfeifer[2]

[1]NanoRobotics Laboratory, Department of Mechanical Engineering,
Carnegie Mellon University
5000 Forbes Ave, Pittsburgh, PA 15213, USA
shuheim@andrew.cmu.edu | +1 412 268 3658
[2]Artificial Intelligence Laboratory, Department of Informatics, University of Zurich
Andreasstrasse 15, 8050 Zurich, Switzerland
{nakajima|pfeifer}@ifi.uzh.ch
[3]Architecture and Sustainable Building Technologies, Department of Architecture,
ETH Zurich
Schafmattstr 32, 8093 Zurich, Switzerland
nagy@arch.ethz.ch

* corresponding author

Abstract

Self-organization is a phenomenon found in biomolecular self-assembly by which proteins are spontaneously driven to assemble and attain various functionalities. This study reports on self-organized behavior in which distributed cm-sized modules stochastically aggregate and exhibit a translational wheeling motion. The system consists of two types of cm-sized water floating modules: a triangular-shaped module that is equipped with a vibration motor and a permanent magnet (termed active module), which can quasi-randomly rove around, and circular modules that are equipped with permanent magnets (termed passive modules). In its quasi-random movement in water, the active module picks up passive modules through magnetic attraction. The contacts between the modules induce a torque transfer from the active module to the passive modules. This results in the rotational motion of the passive modules. As a consequence of the shape difference between the triangular module and the circular module, the passive modules rotate like wheels, being kept on the same edges as the active module. The motion of the active module, as well as the characteristics and behavior of the self-organization process are examined.

keywords
Self-organized behavior, Self-assembly machines, stochasticity, translational wheeling motion, magnetism.

1 Introduction

Self-assembling robotics is a research field that mainly examines spontaneous manufacturing techniques at unreachable domains. The main aim of self-assembling robotics is to achieve a low-cost and efficient fabrication method, high fault-tolerance, and high adaptability, regardless of environmental changes. The approach that this system employs is a so-called bottom-up approach. In this approach, components spontaneously aggregate through local interactions and eventually organize global structures/functionalities. In this way, the systems guarantee high robustness against incidental turbulence and a capability to tolerantly cope with massive parallelism in their aggregation processes. In molecular synthesis, which is arguably the most successful example of self-assembly, some physical conditions are necessary, such as *weak interaction*, *thermal agitation*, and *nucleation*. The mechanisms behind self-assembly are numerous trial and error attempts of collisions until the "right" connection is established. This right connection strength reaches a sustainable level and hence extends beyond the proof reading bias from the turbulent environment. The system utilizes environmental diffusion as a traveling aid and achieves highly efficient assembly matching per unit time. Through such a process, the system gradually shifts to a more energetically stable state. The whole process is fundamentally different than the pick-and-place style, also known as deterministic, of engineering assembly.

[Insert Figure 1]

In order to provide an overview of the current state and trends of self-assembly research, we investigate related research fields, as well as the approach of this study, in Figure 1. For classification, we took the level of the system's homogeneity/heterogeneity in the x-axis, the way modules represent their "states" in the y-axis, and the system's environmental stochastic level in the z-axis. Historically, the first advancement was coined in the field of modular robotics where robots were made from homogeneous sets of modules and, as a result, featured failure tolerance, such as self-repair capability [7, 23]. Self-assembly (SA) robotics used a different approach than modular robotics. SA robotics often incorporate stochasticity in their assembly processes, and modules morphed into targeted configurations under the condition. One of the earliest prototypes was proposed by Murata et al. [21]. Their system consisted of a homogeneous set of units, the ability to develop the assembly patterns, and the ability to self-repair the

formation. A unique approach realizing amoebic locomotion with weakly coupled muti-modules can be found in [16]. The system featured resilient body motions, and showed high adaptability to the environmental changes. Although the introduction of environmental stochasticity varies, such as adding mechanical turbulence to the ground [34], air-jet turbulence [1, 10, 17], and fluid turbulence [24, 32, 35], numerous attempts have been made using this approach. Furthermore, the advancement of hardware allows for the possibility of a derivative field that focuses more on practical implementation, such as the approach that is used for medical surgery/diagnosis [25]. A unique approach to self-disassembly using novel electropermanent magnets is presented in [8]. It is important to note that most of the work subscribes to the so-called bottom-up (stochastic) approach. This approach successfully mimicked bio-molecular activities at the macro scale, proving engineered artifacts' self-replication capability. Although, due to the tendency of employing electronics in the mechanism for internal states, validated capabilities sometimes lack the connection to nature.

On the other hand, there is another approach that employs "mechanical" components for the internal states, which keeps the environment and assembly process stochastic. An early mechanical model for a self-replicating machine in a stochastic environment was attempted by Penrose, in which a provoking mechanical model of natural self-replication was modeled [26]. This research was followed by speculation about the clustering patterns of passive elements and focusing on the role of shape on template and components matching [6], as well as on their time evolution [15]. A group led by Whitesides used a chemistry-inspired approach, where components feature simple (mechanical/chemical) mechanisms. A series of studies was conducted and showed remarkable achievements in the realization of a positional coordinate of molecule-mimetic chemistry [4, 36], circuit functionality [2, 9], reversible aggregation [19], folding structure [3], rotation of magnets [12], and rotation of rotors [11]. Similarly, numerous research efforts have been devoted to the investigation of morphology [31]. Artificial chemicals that can form in several ways depending on the temperature of the system, such as polymers and dimers, were examined in the research completed by Breivik et al. [5]. Different aggregation patterns with various sizes of components were shown in Yamaki et al. [37]. An intelligent self-assembling block, which can represent multiple states of the units' rotational angle, was designed by Tsutsumi et al. [33]. The system can physically express multiple states, conducting exclusive or (XOR) calculation on a 2D plane.

Morphological computation is a notion that reveals the role of players' morphology on various phenomena, regarding them as computation [28]. The focus can be: elucidation of how the particular body works as computation [13,27], and developing a design principle on how to design a new body for a purpose. Self-assembly has had a close connection to this field, especially when the employed modules show strong mechanical features. For instance, differences in segregation patterns in macroscopic modules are reported in [22].

Having considered the mechanisms of biochemical assembly systems, we derive the prerequisite criteria for our approach as follows.

1. **Bottom-up.** The system can potentially handle stochasticity and multi-degree parallelism in the assembly processes, where distributed components autonomously assemble without human intervention.

2. **Mechanical.** To maintain the analogy to biomolecular systems, the module shall ideally be mechanically grounded, which also guarantees scalability. The designed mechanism is expected to provide physical causal paths for the assembly processes. Once a set of experimental conditions is invoked, modules are expected to act independently, following local causal rules imposed by the environment.

3. **Heterogeneity.** Systems that commonly consist of homogeneous components typically attribute failure tolerance against physical damages, although such systems generally lack diversity in their variety of performances. Our interest in this study is having different types of components in an environment as the condition.

4. **Motion by Self-organization.** In contrast to the high loading capacity of carriage components in modules, accomplished functionalities that can be found in literature are mainly concerned with structures or simple electric circuits. One of the major advantages of self-assembly systems is the obtainment of a capability that cannot be attained by a single component. We aim to realize a self-organizing motion that meets the above mentioned conditions.

Having considered the criteria mentioned above, in this study, we focus on attaining translational motion as a self-organized behavior in distributed modules. This kind of motion, which we see in a motor protein in biology, is thought to be crucial when expecting a mobilization of self-assembling components. Translational motion does not only enable a spatial shift of the

components, but also allows them to attain relative positional change of two connected materials (e.g., Kinesins walk on a microtubule and cause muscle contraction). In the following sections, we present our proposed model together with an analytical investigation of a single module's motion by simulations in Section 2. Next we present the attained self-organized behavior in Section 3. We carefully investigate each phenomenon in Section 4 and conclude the study in Section 6.

2 The Model

2.1 Experimental setup

[Insert Figure 2]

The experimental platform was designed to enable the systematic investigation of complex self-assembly phenomenon, which guarantees dissipation and distribution of the system based on [20]. Figure 2 shows (**a**) the modules and (**b**) the experimental environment. The modules floated on water. There were two different types of modules: an active module and a passive module. The active module was equipped with a vibration motor on the top of the base plate, which allowed the module to jiggle and move around in its environment, and a permanent magnet at the bottom for attractive/repulsive interactions (see detail descriptions at Table 1). For the power supply, we opted to supply electricity through a pantograph, which drew current from a metallic ceiling. When voltage was applied to the ceiling plate, current flowed from the pantograph to the vibration motor and then returned to ground via the electrodes that were immersed in conductive water. During the experiments, an NaCl solution was used as conductive water. This water was able to generate sufficient current flow through the chemical reactions: $2\mathrm{NaCl} + 2\mathrm{H_2O} \rightarrow \mathrm{H_2} \uparrow + \mathrm{Cl_2} \uparrow + 2\mathrm{NaOH}$. Due to this setup, all modules received constant power and were lightweight. Generally, the voltage applied to the ceiling determined the level of perturbation introduced into the system. Thus, it can be regarded as a kind of temperature at the macro scale, which can be used as a regulatable parameter. We set up a camera below the water container and observed the modules through the transparent bottom. Table 1 summarizes the components that were equipped on each module.

[Insert Table 1]

2.2 Model of Motion of an Active Module

This section examines the motion of an active module and investigates the influence of a vibration motor. Figure 3 shows a two dimensional model of the active module's motion, where $\boldsymbol{F}_\omega$, $\boldsymbol{F}_n$, $\boldsymbol{F}_r$, $\boldsymbol{F}_f$, $\boldsymbol{F}_v$, θ are the centripetal force of the eccentric mass in a vibration motor, frictional force between the ceiling and the pantograph, resistive force from the ceiling to the pantograph, buoyancy force acting on the module's body, drag force of water to the module's body, and pitch angle of the module, respectively. The relevant values are listed in Table 2.

[Insert Figure 3]

[Insert Table 2]

Let $\boldsymbol{x} = [x, y, z]^T$ be a position vector of the center of mass of the module in a Cartesian coordinate system. Transitional and pitching motions can then be derived from Eq. (1) and Eq. (2), respectively.

$$M\ddot{\boldsymbol{x}} = \boldsymbol{F}_\omega + (M+m)\boldsymbol{g} + \boldsymbol{F}_f + \boldsymbol{F}_r + \boldsymbol{F}_n + \boldsymbol{F}_v \quad (1)$$

$$I\ddot{\theta} = \boldsymbol{r}_\omega \times \boldsymbol{F}_\omega + \boldsymbol{r}_\omega \times m\boldsymbol{g} + \boldsymbol{r}_f \times \boldsymbol{F}_f + \boldsymbol{r}_n \times \boldsymbol{F}_r + \boldsymbol{r}_n \times \boldsymbol{F}_n, \quad (2)$$

where $\boldsymbol{r}_\omega$, $\boldsymbol{r}_f$, $\boldsymbol{r}_n$, and $\boldsymbol{r}_v$ are directional vectors from the center of mass of the module to the action points $\boldsymbol{F}_\omega$ ($m\boldsymbol{g}$), $\boldsymbol{F}_f$, $\boldsymbol{F}_n$ ($\boldsymbol{F}_r$), and $\boldsymbol{F}_v$, respectively. M, m, and I are the mass of the module body, mass of the eccentric weight in a vibration motor, and moment of inertia around the center of the module's mass, respectively.

The directional vectors can be represented as:

$$\boldsymbol{r}_\omega = L_c[-\sin(\theta), 0, \cos(\theta)]^T + L_a\cos(\omega t)[-\cos(\theta), 0, -\sin(\theta)]^T \quad (3)$$

$$\boldsymbol{r}_f \approx [\frac{L_x\theta}{3\arctan(L_z/L_x)}, 0, \frac{L_x\theta^2}{3\arctan(L_z/L_x)}]^T \quad (4)$$

$$\boldsymbol{r}_n = [-\tan(\theta)(L_d - z), 0, L_d - z]^T \quad (||\boldsymbol{r_n}|| \leq L_l), \quad (5)$$

where we simplify that the origin of the floating force comes on the horizontal center line of the module, which is proportionally distant from the center of mass to the pitch angle (θ).

Each force can be simplified as:

$$\boldsymbol{F}_{\omega} = m\omega^2 L_a[\cos(\omega t)\cos(\theta), \sin(\omega t), \cos(\omega t)\sin(\theta)]^T \tag{6}$$

$$\boldsymbol{F}_{f} \approx [0, 0, 2\rho g L_x^2(-z + L_z\cos(\theta))]^T \tag{7}$$

$$\boldsymbol{F}_{r} = \begin{cases} [0,0,0]^T & (||\boldsymbol{r_n}|| > L_l) \\ -k(L_l - ||\boldsymbol{r_n}||)[0,0,1]^T & (||\boldsymbol{r_n}|| \leq L_l) \end{cases} \tag{8}$$

$$\boldsymbol{F}_{n} = \begin{cases} [0,0,0]^T & (||\boldsymbol{r_n}|| > L_l) \\ sign(r_n)\mu||\boldsymbol{F_r}||[1,0,0]^T & (||\boldsymbol{r_n}|| \leq L_l) \end{cases} \tag{9}$$

$$\boldsymbol{F}_{v} \approx -c[\dot{x}, \dot{y}, \dot{z}]^T, \tag{10}$$

where k is the spring constant of the pantograph, μ is the kinetic frictional coefficient, and c is the coefficient of the water's drag force. Note that the flickering contact of the pantograph to the ceiling caused by the vibration motion added some fluctuations to the current flow through the motors. However, since the drive of the motor is mainly affected by the supplied power that can be temporarily averaged, we believe that the influence of perturbation is negligible and does not incorporate into the model. Note that the rotational speed of the eccentric mass is quasi proportional to the voltage applied. As this speed increased, the modules moved faster and there were stronger collisions between them.

[Insert Figure 4]

Figure 4 illustrates the numerically solved simulation results of the motion of an active module. In the simulation, initial values were set as $[x,\ x',\ z,\ z',\ \theta,\ \theta'] = \mathbf{0}$. We compare the results by varying the rotational frequency of the vibration motor as 12000 rpm, 13000 rpm, and 14000 rpm, which roughly corresponds to 5.5 V, 6.0 V, and 6.5 V of the applied voltage to the ceiling. These values are derived by referring to the plot in the data sheet of the product.

Figure 4 **a** shows the time evolution of x and z positions of a module. In addition to the high frequency oscillations seen in the x-direction, which is caused by the vibrational motion, long periods of oscillations of about 10 Hz in z-direction can be recognized in each case. Moreover, the magnitudes of this low frequency oscillation along z-direction vary depending on the rotation

speeds of the vibration motors. Translational motion along x-direction, especially in a longer period (e.g., 10 s), was observed in each case. However, these values were usually small (e.g., not more than 1.5 cm in 10 seconds) compared to the experimentally obtained data and were not easily distinguishable from the accumulated numerical errors, which are not discussed in this research.

Figure 4 **b** shows the time evolution of the pitch angle of a module (θ). Note that the maximum angle in practice is $\pm 14.25\,^\circ$ (± 0.249 rad), which happens when an edge of the bottom surface of the module was about to be detached from the water surface, or the top surface of the module was about to go below the water surface. The simulation result showed two different scale frequencies. In addition to the approximate 200 Hz high frequency wave caused by the vibrational motion, the module tilted alternately to the opposite directions approximately every 0.13 s. Faster vibration did not only cause an increase in high frequency oscillation, but also in low frequency oscillation.

2.3 Magnetic interaction

The magnets on the modules provided long range interaction between the modules as follows. Consider two magnetic dipoles $\boldsymbol{m}_i$ and $\boldsymbol{m}_j$ $(i, j \in \mathbb{N}, i \neq j)$ at the center of a mass of modules i and j separated by a distance $r_{ji} \gg d$ (d : side length of the magnet). The magnetic flux density at the position of $\boldsymbol{m}_i$ created by $\boldsymbol{m}_j$ can be described with a position vector $\boldsymbol{r}_{ji}$ as:

$$\boldsymbol{B}_{ij} = \frac{\mu_0}{4\pi}\left[\frac{3(\boldsymbol{m}_j \cdot \boldsymbol{r}_{ji})\boldsymbol{r}_{ji}}{r_{ji}^5} - \frac{\boldsymbol{m}_j}{r_{ji}^3}\right], \tag{11}$$

where $\mu_0 = 4\pi \times 10^{-7}$ Tm/A is the permeability of free space.

The magnetic force, torque, and energy acting on $\boldsymbol{m}_1$ due to $\boldsymbol{m}_2$ are respectively given as:

$$\boldsymbol{F}_{ij} = (\boldsymbol{m}_i \cdot \nabla)\,\boldsymbol{B}_{ij} \tag{12}$$

$$\boldsymbol{\tau}_{ij} = \boldsymbol{m}_i \times \boldsymbol{B}_{ij} \tag{13}$$

$$U_{ij} = -\boldsymbol{m}_i \cdot \boldsymbol{B}_{ij}. \tag{14}$$

Since the magnets were mounted onto the modules along the z-axis, we consider them either as

parallel or anti-parallel for the interaction. Then, Eq. (13)–(14) is simplified as follows:

$$\boldsymbol{F}_{ij} = \sigma_{ij} \frac{3\mu_0}{4\pi} \frac{m_i m_j}{r_{ij}^5} \boldsymbol{r}_{ji}, \qquad \sigma_{ij} = \frac{\boldsymbol{m_i} \cdot \boldsymbol{m}_j}{|\boldsymbol{m}_i||\boldsymbol{m}_j|} \tag{15}$$

$$\boldsymbol{\tau}_{ij} = \mathbf{0}, \tag{16}$$

$$U_{ij} = \sigma_{ij} \frac{\mu_0}{4\pi} \frac{m_i m_j}{r_{ij}^3}, \qquad \sigma_{ij} = \frac{\boldsymbol{m_i} \cdot \boldsymbol{m}_j}{|\boldsymbol{m}_i||\boldsymbol{m}_j|}. \tag{17}$$

Namely, these expressions imply that the attraction and repulsion of the two magnets were determined by the orientations and that magnetic force simply decayed in inverse proportion to distance to the power of four ($\propto r^{-4}$). Torque acting on a single module is zero. This is one of the advantages of the system, since, when the interactions of modules are further developed, we only need to account for the distances.

We can determine the total potential energy of the system as

$$U_{total} = \sum_{i>j} U_{ij}. \tag{18}$$

Finally, we normalized the energy as $U'_{total} \equiv U_{total}/(\frac{\mu_0}{4\pi} m^2)$, assuming that all of the magnets are equally magnetized as ($m_i = m_j = m$, for $\forall i, j$). The system minimizes the potential magnetic energy over time. The value and the terrain of the function articulate the preferable configuration and stability of a system.

3 Self-organizing Translational Wheeling Behavior

Figure 5 **a-i** shows a behavior that was typically observed in the experiments. As an initial condition, we manually placed an active module at the center of the container and positioned three passive modules (colored green) along the wall so that they were equally distributed (Figure 5 **a**). Once a voltage was applied, the following actions took place: a translational motion of the active module, contact to the passive module (the 1st assembly), and rotation of the passive module on an edge of the active module (as soon as an assembly occurs, the circular module begins to rotate, Figure 5 **b**), wall following behavior driven by the active triangle module (Figure 5 **c-d**), the 2nd and the 3rd assembly (2nd: Figure 5 **c**, 3rd: Figure 5 **e**), rotational movement (Figure 5 **f**, **g**), and wall following (Figure 5 **h-i**). The rotational movements were observed when at least one passive module was attached to an active module, and the whole body did not have any contact with the wall.

[Insert Figure 5]

The assembly motion, the rotational movement, and the wall following behaviors can also be recognized in Figure 5**j**, where the time evolution of x-positions of all the modules are displayed. The rotation of the whole body can be recognized as 120°-phase delay (highlighted in dotted boxes), and the wall following behavior can be seen as coherent phases (highlighted in dotted boxes). These dynamical motions are thought to be attractors when there is no influence from the wall.

The transition of the system's potential magnetic energy is shown in Figure 5**k**. The energy drops can be identified when assemblies occur. It is shown that the energy is mainly consumed for the assembly and has little to do with the motion. Compared to the rotational phase, the wall following phase shows periodic rises and falls in the energy transition. This is because the active module often changes its relative position to the "wheeling" two passive modules: the active module occasionally "sank" into passive modules. Nevertheless, the system maintains a stable translational motion, as can be seen in Figure 5**j**, proving the intrinsic robustness of the model.

In the following section, we respectively investigate different observed behaviors classifying into assembly process (Section 4.1), rotational movement (Section 4.2), and wall following (Section 4.3).

4 Investigations

4.1 Self-assembly Process

Assemblies were mainly managed by magnetic attraction, though it has little influence when modules are apart. An active module has to rove around the field and have physical contact with a passive module. We plotted two examples of the trajectory in Figure 6, where an active module picked up two passive modules (the 3rd assembly normally takes long and is, as a result, excluded from the plot). The trajectories clearly show distinct correlated movements of passive modules when assembly occurs. This shows that the influence of magnetic attractions is mainly affective when two modules are in contact.

[Insert Figure 6]

Figure 7 **a** shows the time that was needed for the 1st and the 2nd assembly. Note that we define the trials whose assembly interval (1st to 2nd) took more than 30 s as "trapped" trials and they were eliminated from the statistics. Such trials were observed in 6 out of the 21 trials (success rate=71.4 %). The average time of the 1st assembly was 2.92 s (±2.53 s) and the average time of the 2nd was 11.88 s (±6.38 s).

[Insert Figure 7]

It is worth noting that the 2nd assembly took longer in general and the variance was high. The reason for this is that their magnetic fields cancelled each other out, making other magnetic interactions weaker compared to a single module-module interaction. See also Figure 8 and its discussion below. We observed typical trapped states in Figure 7 **b**,**c**. The states of an active (vibration motor equipped) triangle and a passive circle driven by the active module pulled each other in opposite directions and, consequently, made them stay in the same place (Figure 7 **b**). This happened because there is only one active module. As a result, the convergence to the local minimum state should be avoided if there is another active module. Also, an observed different locally stable configuration is illustrated in Figure 7 **c**, where a carried passive module pushed other passive modules and was prevented from connecting to the active module.

[Insert Figure 8]

In order to see the influence of the 1st assembly, we visualized terrains of magnetic potential energy of different assembly stages in Figure 8. We place modules as displayed: only the active module exists in the container (**a**), one passive module is attached to the active module (**b**), two passive modules are attached (**c**), and three passive modules are attached (**d**). The streamlines are derived based on (18), representing the gradient decay of U_{total}. Namely, it tells the paths of an additional passive module in the field. It can be seen that, as the assembly process proceeds from Figure 8 **a** to Figure 8 **d**, the attractive region of the active module drastically decreases. In Figure 8 **a**, a passive module is attracted omni-directionally; in Figure 8 **b**, due mainly to the boundary effect, the attractive region decays to almost half of the size (ideally a second passive module should reach to the active module following the path); in Figure 8 **c**, the attachment of the second passive tile further decreases the attractive region; and in Figure 8 **d**,

the complete assembly does not provide a significant attractive region. The comparison between Figure 8 **a** and Figure 8 **d** tells us that, while in **a**, it is omni-directionally attractive and it is omni-directionally repulsive in **d**. That means that, if another group exists like the one in **d** in the field, they repel each other.

4.2 Rotation of a group

A rotational motion was observed when at least one passive module had a connection to an active module, while none of the modules was touching the container boundary. Figure 9 **a**, **b** shows the experimentally obtained time evolutions of the rotational motions' trajectories.

[Insert Figure 9]

The rotational velocities were 1.14 rad/s in Figure 9 **a**, and 0.70 rad/s in Figure 9 **b**. The directions of rotation were the same all the time and determined by the rotational direction of the vibration motor. The rotational speeds vary, especially in the case of Figure 9 **b**. Being hindered in its motion, the passive modules occasionally contacts the boundary. The lasting times vary, due to the relative positions of the whole group to the boundary, while the motion stably lasted.

Rotation of an assembled group (at least one passive and one active module) arises due to the conservation of the angular momentum since no external torque is applied to the cluster. The frictional collisions between the modules induce a friction force, which in turn generates a torque in both modules in the same direction, leading to a non-zero total torque on the cluster. This non-zero torque must be balanced to fulfill the conservation of the angular momentum, and thus yield the observed rotation of the cluster.

4.3 Wall following and morphology dependence

Wall following behaviors were frequently observed in the experiments, though they did not necessarily occur when passive modules acted as wheels. This behavior was performed either by an active triangle module (Figure 10 **b**) or was indirectly performed through two passive modules (Figure 10 **c**). The requirement of this phenomenon is a larger capillary force between the wall and the modules having contact(s) to the wall. We roughly estimate the capillary force using magnets; measuring the distance of which causes detachment of a module placed on a

wall of the container. We use the same strength of magnets as listed in Table 2 and derive the average distance of 3.73 cm with standard deviation 0.25 cm. Taking the magnetization into account, we obtain 0.26 N as the average capillary force between a module and the container.

[Insert Figure 10]

We examined the speed of the wall following behaviors depending on different applied voltages show in Figure 10 **a**. In general, increases in velocities were recognized as increases in applied voltages in both cases (4.67 cm/s to 10.07 cm/s with triangle, and 7.68 cm/s to 10.22 cm/s with bike). However, the speeds of the triangle and bike configurations under 7 V were not significantly different. Note that the velocities can be changed to negative by applying negative voltage to the system.

We further examined the effect of morphology by magnifying the size of passive modules (Figure 10 **d**). Interestingly, the speed decayed in both conditions, 5.5 V and 7.0 V, compared to normal passive modules (18.1% decrease at 5.5 V, and 12.9% decrease at 7.0 V from the normal bike configuration, respectively). This suggests that there exists an appropriate size match between active and passive modules.

5 Discussions

5.1 Reliability to the environmental condition changes

The reliability of the presented system against environmental condition changes (size of the container, the applied voltage, or the viscosity of the water) is an important issue to be discussed. These conditions have not been systematically investigated in experiments, but will be discussed based on our observations. The container size may influence the assembly time and the capillary effect. Given that the motion of an active module can be regarded as a quasi-random walk and obeys diffusion law, the required time to travel a distance, L, is proportional to L^2. This means that the assembly time is expected to increase with respect to the size of the container. The size or more precisely the curvature (shape) of the container affects the contact surface area between a module and the container. As we described, the capillary attraction between a module and the container wall enabled reliable wall following behavior, therefore the lack of this force will most likely disable wall following behavior and increase the chance of a rotational motion. The

applied voltage is a significant factor in the system's behavior. First, if the applied voltage is too high, i.e., the agitation level of an active module is too high to maintain a connection to a passive module, the system cannot aggregate [20]. Conversely, an application of a too low voltage will cause a slow translational motion of an active module, and lead to longer assembly time. The influence of other parameters, such as viscosity, temperature, or the conductivity of the water would require an extended study because they are interdependent and there are many practical restrictions. The water viscosity can be continuously altered by temperature to some degree, but it also affects the conductivity of the water. The prediction of behavior becomes difficult if these conditions are significantly changed. Some predictable changes exist, such as decay in translational motion of an active module as indicated in Eq. (10) with a constant of viscosity, if the applied change is minor. Unless capillary force is affected, we suppose that constant observation of wall following behavior is expected.

5.2 Possibility of different combination of modules

Scalability with respect to the number of modules is an important factor to be taken into account when designing self-organization systems. However, the prediction is not trivial even when adding one more module to the system. To observe this point, we attempted the experiment with different sets of modules: two active and two passive module sets, and two active and three passive module sets. The most recognizable pattern was a group configuration consisting of two active and two passive modules forming a lattice structure with modules aligned alternately, but showing no noteworthy behavior. To attain efficient and selective assembly, modules should intrinsically feature hierarchical functions acting logically to the input, e.g. a module prohibits further magnetic interaction when establishing an ideal connection. To date, only a few studies have investigated mechanically attained internal states that enable logical reactions [15, 26, 29].

Related to this point, Figure 8 provides a unique insight on how simple modules could attain "computation". It shows that the maximum number of passive modules that can connect to an active module is three (no matter how many passive modules exist). This is determined by the combination of morphologies of an active module and a passive module, where the increment of the number of connected passive modules causes reduction of attractive region. Instead, this can be done with internal states as introduced in [29]. In this sense, morphology can be defined through an internal state and the module's outline.

5.3 Design of the shape and function of the self-organization system

Unlike static self-assembly systems where the targets are mostly "structures", dynamic self-assembly, self-organization system, and self-assembly robotics often aim at: (1) "Motion", which can be either positional motion (such as translational or rotational), or morphological motion (such as elongation or bending), and (2) "Function", especially those which can be distinguishable from motion, such as metabolism or self-reproduction and whose notions are often taken from biology. Designing a structure entails many features, and thus requires attention when designing. For example, the targeted attribute to yield can be the length, size, stiffness, or topology. The regulation between the autonomy of a module and capability of the system is crucial for attaining a motion or function. In this regard, the level of a system's heterogeneity is a crucial topic variable to be considered when designing a self-organization system. The model presented here consists of two different shaped modules. The wall following motion presented here is a good example that shows when fitting types of modules match, they exhibit advanced behavior even with simple modules. The regulation between heterogeneity and the autonomy is often a trade-off issue, and the optimized position needs to be derived. If the aimed motion or function is already clear, which is usually a rare case (the "library" of such patterns has been fulfilled to a good degree), an evolutional optimization method may suit, e.g., if the aimed behaviors is the swimming speed [30] or locomotion speed [14, 18]. However, the difficulty here is always how to objectively find and set a good fitness function.

6 Conclusion

This paper reports a self-organizing translational motion that is performed by a set of water-floating self-assembly modules. The system features the least hardware implementation for the operation, namely one motor but no sensors, and shows reliable assembly and a stable wheeling behavior. During the experimental run, a floating module with a vibration motor (active module) roves around the area, and eventually picks up passive modules through magnetic attraction. By retaining contacts with multiple passive modules, an active triangular module transmits torque to the passive modules, inducing rotation of the passive modules, and consequently utilizes them as wheels. We classify the entire self-organizing behavior as follows: 1) self-assembly phase, 2) rotational motion phase, and 3) wall following phase. We also carefully investigated the associated characteristics. We further studied the influence of morphology,

which, in this research, is the size of passive modules that act as wheels. This study provides insight into how morphology in assembled structures augments the "summed-up" functionalities of individual components of the structure.

Acknowledgment

The most of the topics discussed in Section 5 are prompted by the reviewers' suggestion. We sincerely thank the reviewers for inputs. This work was partially supported by a Swiss National Science Foundation Fellowship PBZHP2-133472.

References

1. Bishop, J., Burden, S., Klavins, E., Kreisberg, R., Malone, W., Napp, N., & Nguyen, T. (2005). Programmable parts: A demonstration of the grammatical approach to self-organization. *IEEE/RSJ International Conference on Intelligent Robots and Systems (IROS)*, pp. 3684–3691.

2. Boncheva, M., Ferrigno, R., Bruzewicz, D. A., & Whitesides, G. M. (2003). Plasticity in self-assembly: Templating generates functionally different circuits from a single precursor. *Angewandte Chemie International Edition*, 42, 3368–3371.

3. Boncheva, M., Andreev, S. A., Mahadevan, L., Winkleman, A., Reichman, D. R., Prentiss, M. G., Whitesides, S., & Whitesides, G. M. (2005). Magnetic self-assembly of three-dimensional surfaces from planar sheets. *Proceedings of the National Academy of Sciences*, 102(11), 3924–3929.

4. Bowden, N., Terfort, A., Carbeck, J., & Whitesides, G. M. (1997). Self-assembly of mesoscale objects into ordered two-dimensional arrays. *Science*, 276(5310), 233–235.

5. Breivik, J. (2001). Self-oranization of template-replicating plolymers and the spontaneous rise of genetic information. *Entropy*, 3, 273–279.

6. Cohn, M. B., & Kim, C.-J. (1991). Self-assembling electrical networks: An application of micromachining technology. *International Conference on Solid-State Sensors and Actuators*, pp. 490–493.

7. Fukuda, T., & Kawauch, Y. (1990). Cellular robotic system (CEBOT) as one of the realizations of self-organizing intelligent universal manipulator. *IEEE International Conference on Robotics and Automation (ICRA)*, pp. 662–667.

8. Gilpin, K., Knaian, A., & Rus, D. (2010). Robot pebbles: One centimeter module for programmable matter through self-disassembly. *IEEE International Conference on Robotics and Automation (ICRA)*, pp. 2485–2492.

9. Gracias, D. H., Tien, J., Breen, T. L., Hsu, C., & Whitesides, G. M. (2000). Forming electrical networks in three dimensions by self-assembly. *Science*, 289(5482), 1170–1172.

10. Griffith, S., Goldwater, D., & Jacobson, J. (2005). Robotics: Self-replication from random parts. *Nature*, 437, 636.

11. Grzybowski, B. A., Radkowski, M., Campbell, C. J., Lee, J. N., & Whitesides, G. M. (2004). Self-assembling fluidic machines. *Applied physics letters*, 84, 1798–1800.

12. Grzybowski, B. A. Stone, H. A., & Whitesides, G. M. (2000). Dynamic self-assembly of magnetized, millimetre-sized objects rotating at a liquid-air interface. *Nature*, 405, 1033.

13. Hauser, H., Ijspeert, A. J., Füchslin, R. M., Pfeifer, R., & Maass, W. (2011). Towards a theoretical foundation for morphological computation with compliant bodies. *Biological Cybernetics*, 105, 355–370.

14. Hiller, J., & Lipson, H. (2012). Automatic design and manufacture of soft robots. *IEEE Transactions on Robotics*, 28, 457–466.

15. Hosokawa, K., Shimoyama, I., & Miura, H. (1994). Dynamics of self-assembling systems: Analogy with chemical kinetics. *Artificial Life*, 1, 413–427.

16. Ishiguro, A., Shimizu, M., & Kawakatsu, T. (2006). A modular robot that exhibits amoebic locomotion. *Robotics and Autonomous Systems*, 54, 641–650.

17. Klavins, E. (2007). Programmable self-assembly. *IEEE Control System Magazine*, 27, 43–56.

18. Lipson, H., & Pollack, J. B. (2000). Automatic design and manufacture of artificial lifeforms. *Nature*, 406, 974–978.

19. Mao, C., Thalladi, V. R. Wolfe, D. B., Whitesides, S., & Whitesides, G. M. (2002). Dissections: Self-assembled aggregates that spontaneously reconfigure their structures when their environment changes. *Journal of the American Chemical Society*, 124(49), 14508–14509.

20. Miyashita, S., Göldi, M., & Pfeifer, R. (2011). How reverse reactions influence the yield rate of stochastic self-assembly. *International Journal of Robotics Research*, 30, 627–641.

21. Murata, S., Kurokawa, H., & Kokaji, S. (1994). Self-assembling machine. *IEEE International Conference on Robotics and Automation (ICRA)*, pp. 441–448.

22. Nakajima, K., Ngouabeu, A. M. T., Miyashita, S., Göldi, M., Füchslin, R. M., & Pfeifer, R. (2012). Morphology-induced collective behaviors: Dynamic pattern formation in water floating elements. *PLoS ONE*, 7(6), e37805.

23. Nakano, K., Uchihashi, S., Umemoto, N., & Nakagama, H. (1994). An approach to evolutional system. *First IEEE Conference on Evolutionary Computation (CEC)*, pp. 781–786.

24. Neubert, J., Cantwell, A. P., Constantin, S., Kalontarov, M., Erickson, D., & Lipson, H. (2010). A robotic module for stochastic fluidic assembly of 3d self-reconfiguring structures. *IEEE International Conference on Robotics and Automation (ICRA)*, pp. 2479–2484.

25. Oetomo, D., Daney, D., Harada, K., Merlet, J.-P., Menciassi, A., & Dario, P. (2009). Topology design of surgical reconfigurable robots by interval analysis. *IEEE International Conference on Robotics and Automation (ICRA)*, pp. 3085–3090.

26. Penrose, L. S. (1959). Self-reproducing machines. *Scientific American*, 200-6, 105–114.

27. Pfeifer, R., & Bongard, J. C. (2007). *How the body shapes the way we think*. The MIT Press. Cambridge, MA.

28. Pfeifer, R., Iida, F., & Gomez, G. (2006). Morphological computation for adaptive behavior and cognition. *International Congress Series*, 1291, 22–29.

29. Saitou K., & Jakiela, M. J. (1995). Automated optimal design of mechanical conformational switches. *Artificial Life*, 2, 129–156.

30. Sims, K. (1994). Evolving 3D morphology and behavior by competition. *Artificial Life IV*, pp. 28–39.

31. Stambaugh, J., Lathrop, D. P. Ott, E., & Losert, W. (2003). Pattern formation in a monolayer of magnetic spheres. *Pysical Leview E*, 68, 026207–1–026207–5.

32. Michael, T., & Lipson, H. (2010). Fluidic manipulation for scalable stochastic 3d assembly of modular robots. *IEEE International Conference on Robotics and Automation (ICRA)*, pp. 2473–2478.

33. Tsutsumi, D., & Murata, S. (2007). Multistate part for mesoscale self-assembly. *SICE Annual Conference*, pp. 1–6.

34. White, P., Kopanski, K., & Lipson, H. (2004). Stochastic self-reconfigurable cellular robotics. *IEEE International Conference on Robotics and Automation (ICRA)*, pp. 2888–2893.

35. White, P., Zykov V., Bongard, J., & Lipson, H. (2005). Three dimensional stochastic reconfiguration of modular robots. *International Conference on Robotics Science and Systems (RSS)*, pp. 161–168.

36. Wolfe, D. B., Snead, A., Mao, C., Bowden, N. B., & Whitesides, G. M., (2003). Mesoscale self-assembly: Capillary interactions when positive and negitive menisci have similar amplitudes. *Langmuir*, 19(6), 2206–2214.

37. Yamaki, .M, Higo, .J, & Nagayama, K. (1995). Size-dependent separation of colloidal particles in two-dimensional convective self-assembly. *American Chemical Society*, 11, 2975–2978.

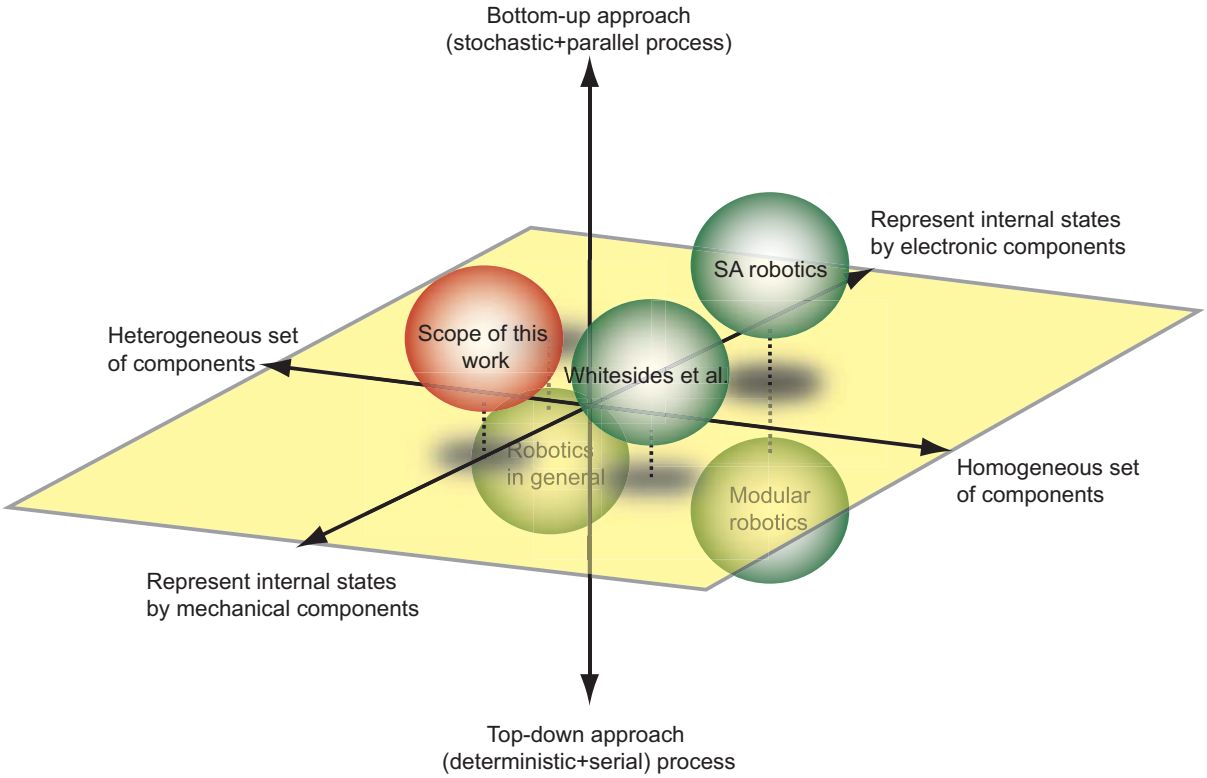

Figure 1: Related research fields are as follows: Homogeneity of components (x-axis), module mechanism of internal states (y-axis), and approaches (z-axis).

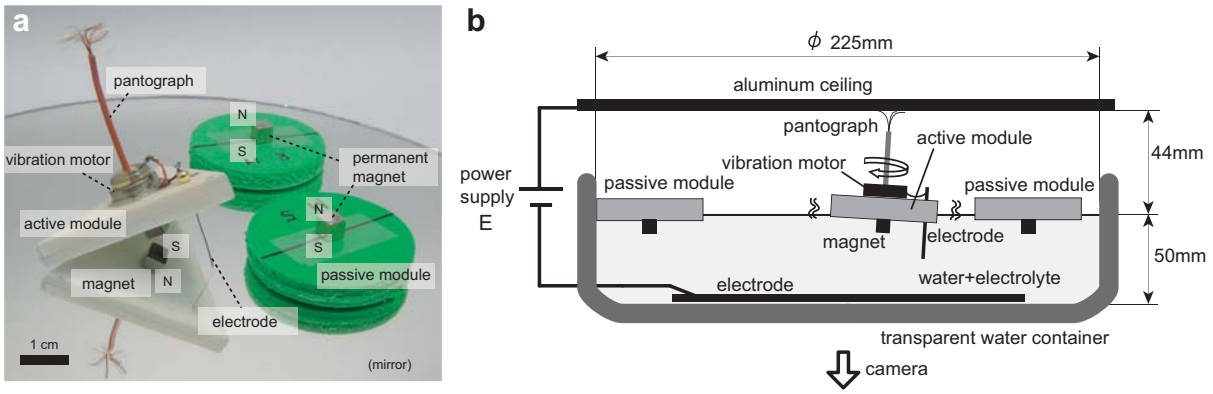

Figure 2: Designed modules and experimental setup. **a**: active module (white triangular module) and passive modules (green circular modules). **b**: Outlook of the experiment.

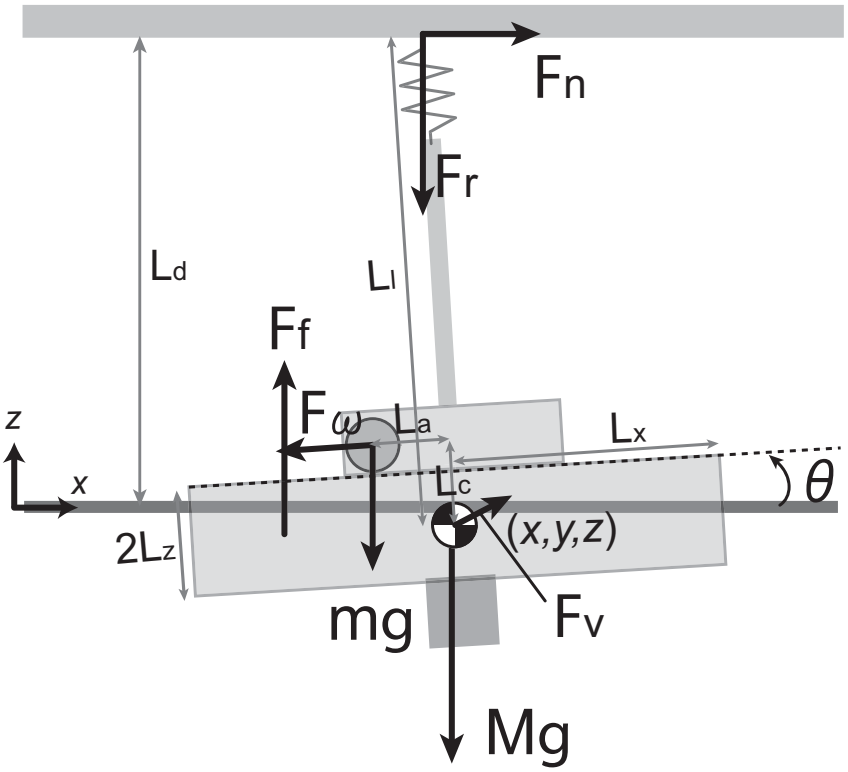

Figure 3: Schematic of a single module. $\boldsymbol{F}_\omega$, $\boldsymbol{F}_n$, $\boldsymbol{F}_r$, $\boldsymbol{F}_f$, $\boldsymbol{F}_v$, θ are centripetal force, frictional force, resistive force, buoyancy force, drag force, and pitch angle of the module, respectively. The descriptions of relevant variables are listed in Table 2.

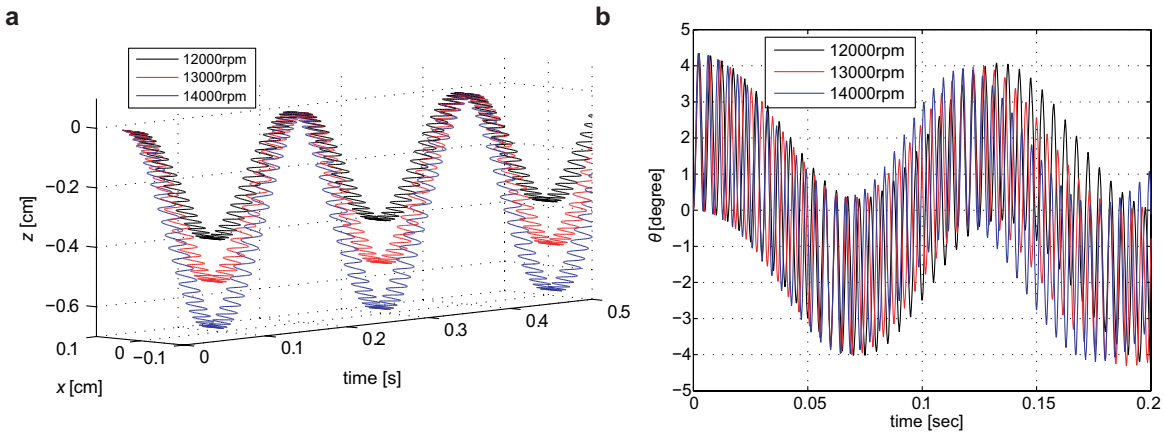

Figure 4: Simulation Results of motion of an active module. **a:** time evolution of x and z motion. **b:** time evolution of pitch angle of the module. We varied the rotational frequency of the vibration motor as 12000 rpm, 13000 rpm, and 14000 rpm, which approximately corresponded to 5.5 V, 6.0 V, and 6.5 V of the applied voltage to the ceiling.

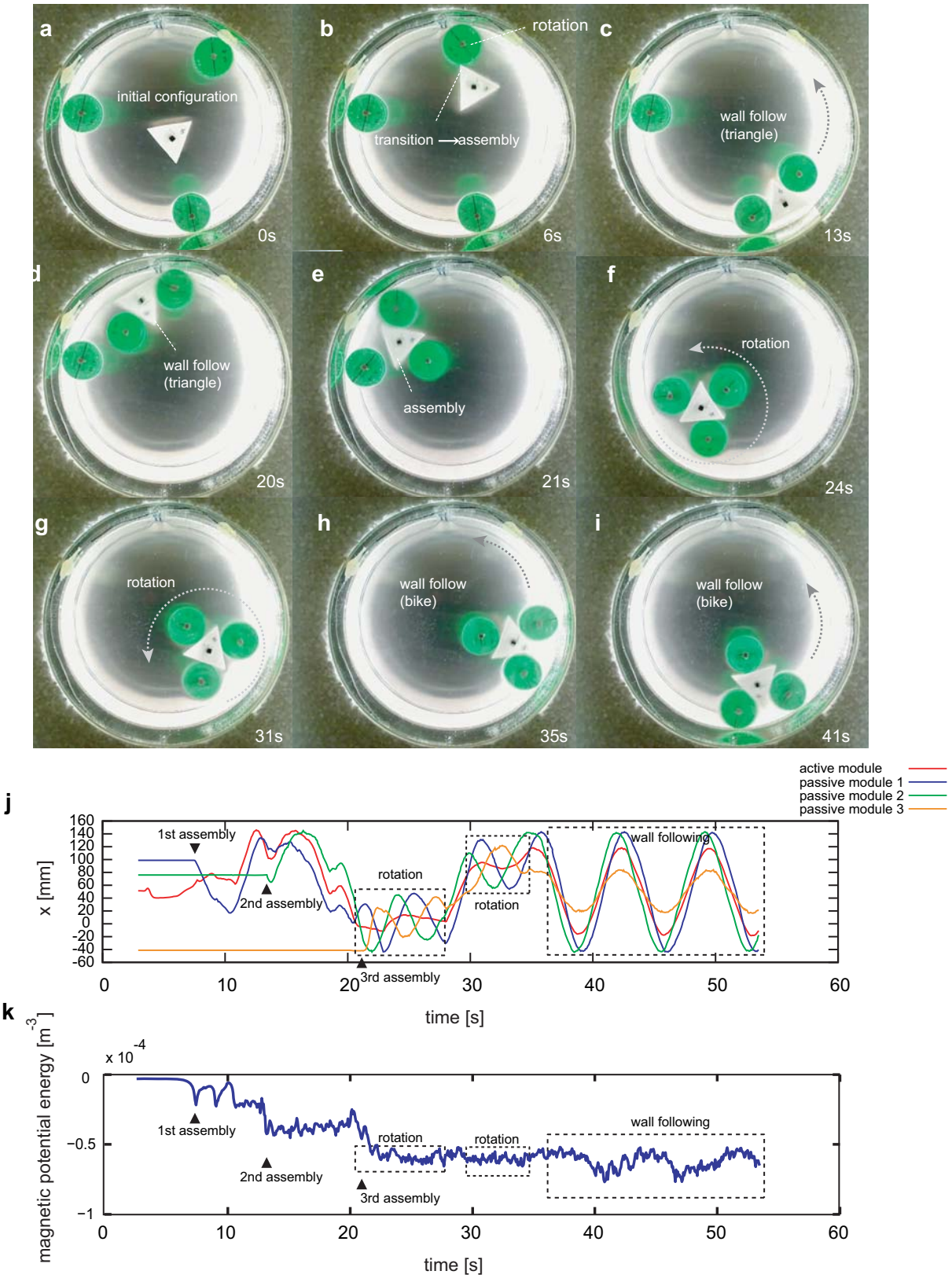

Figure 5: Representative experimental run, consisting of assembly motion (1st assembly, **b**), wall following behavior driven by active triangle module (**c**-**d**), 3rd assembly (**e**), rotational movement (**f**, **g**), and wall following indirectly managed by passive modules (**h**-**i**). Time evolution of x-positions of all the modules (**j**) and normalized magnetic potential energy (**k**).

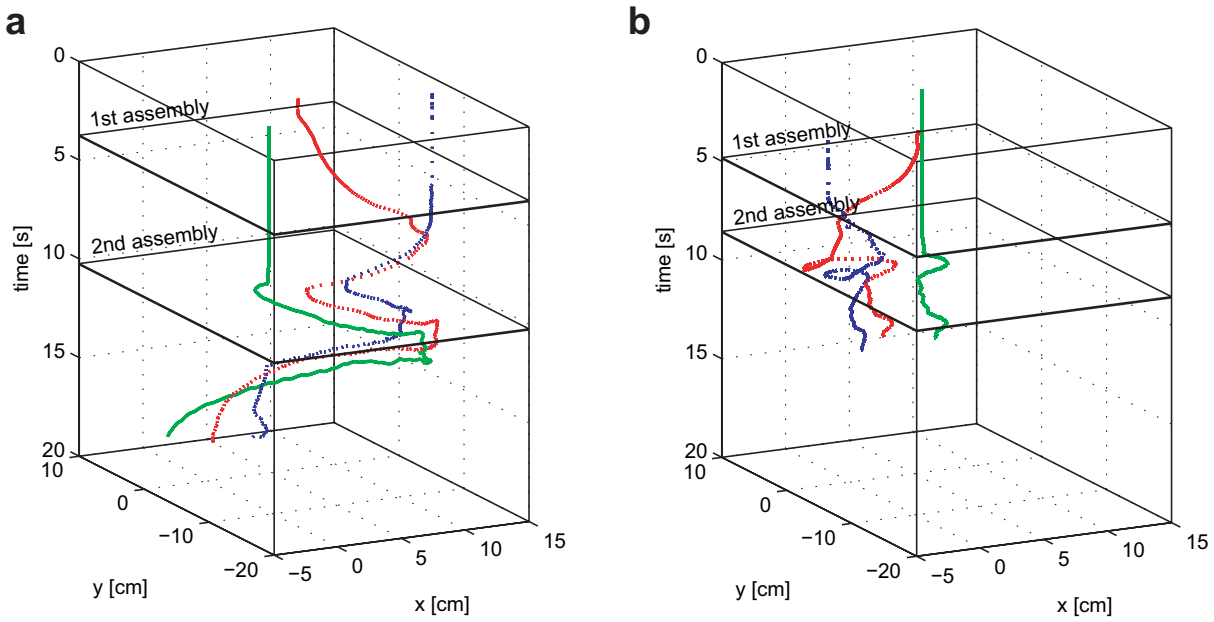

Figure 6: Assembly process (trajectory). **a** and **b** are randomly chosen different trials, where one can see the difference in time taken and correlated motions after assembly.

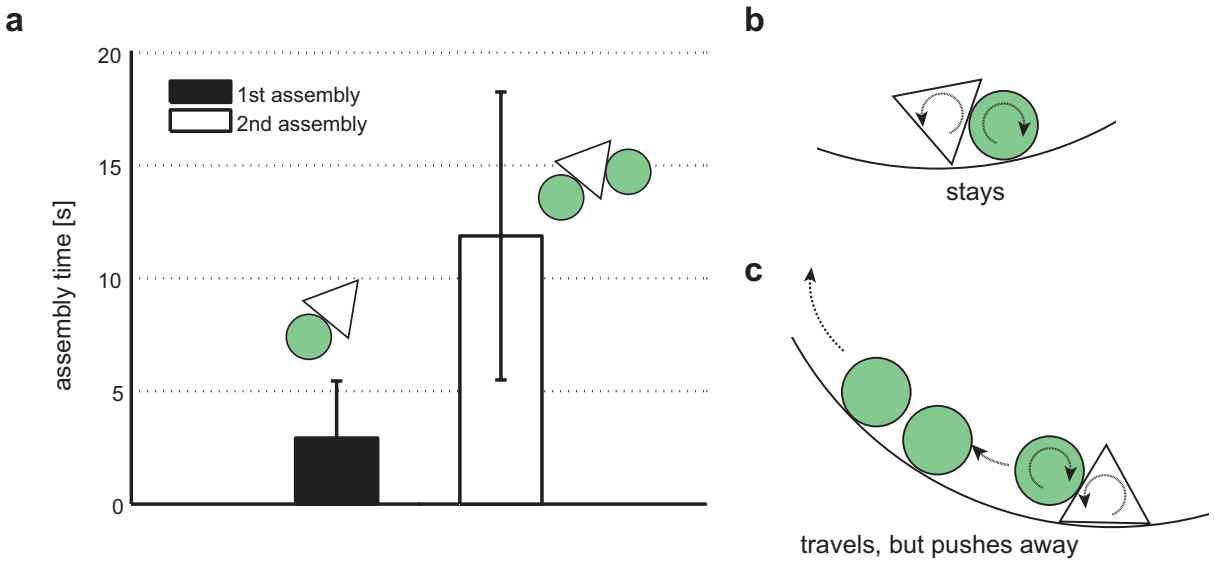

Figure 7: Assembly time, (7.0V, n=15). **a:** Assembly time taken for 1st and 2nd assembly. **b,c:** typical "trapped" situations.

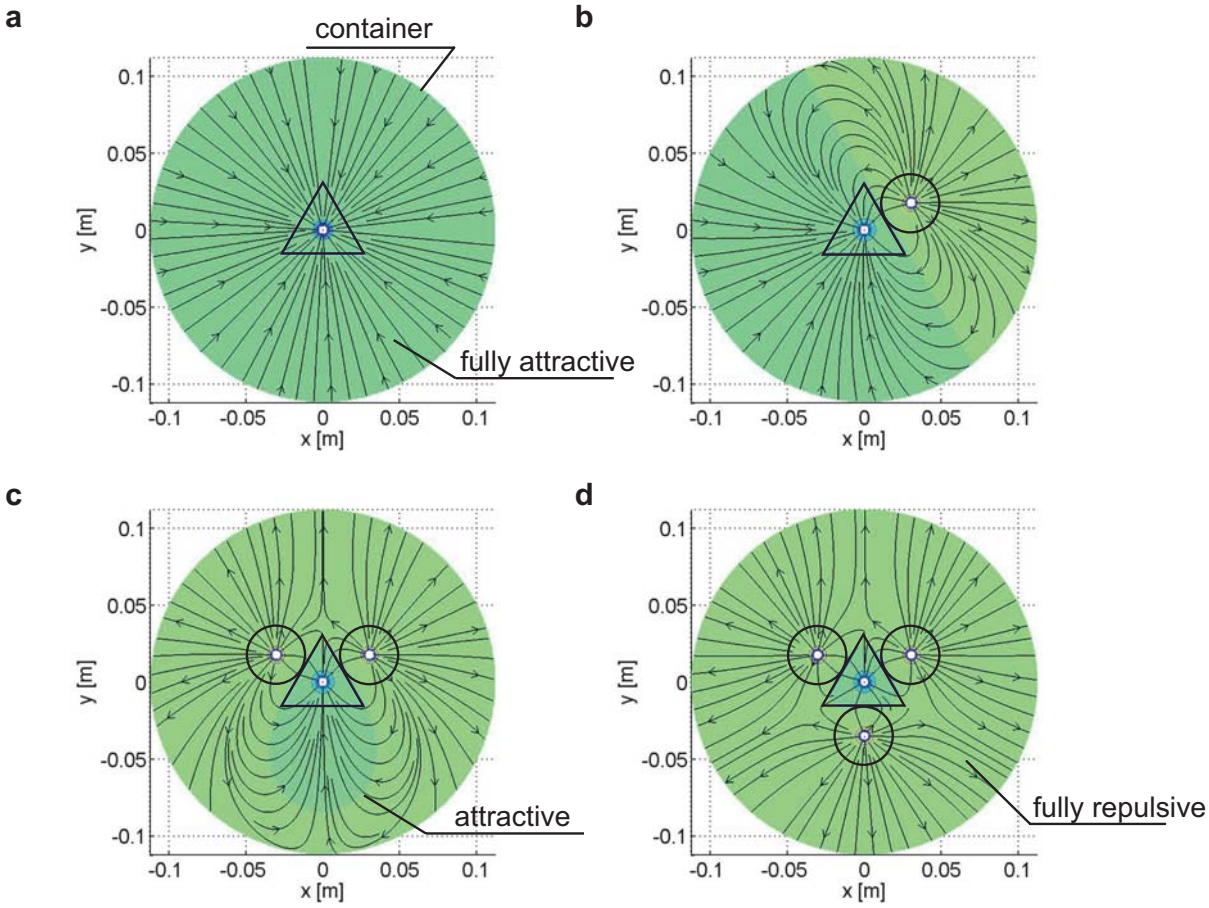

Figure 8: Attractive regions depending of different assembly stages: only the active module exists in the container (**a**), one passive module is attached to the active module (**b**), two passive modules are attached (**c**), three passive modules are attached (**d**).

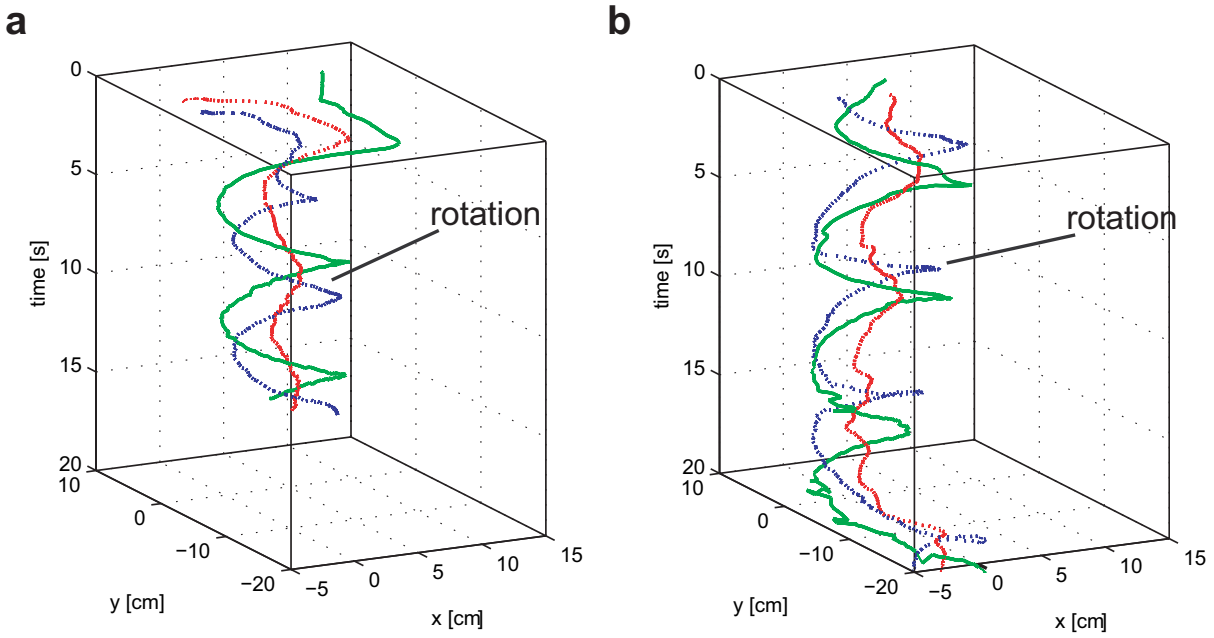

Figure 9: Rotational motion (trajectory and illustration). **a** and **b** are from different trials. The rotational behavior is stably observed, and it usually lasts until the group hits the wall of the container.

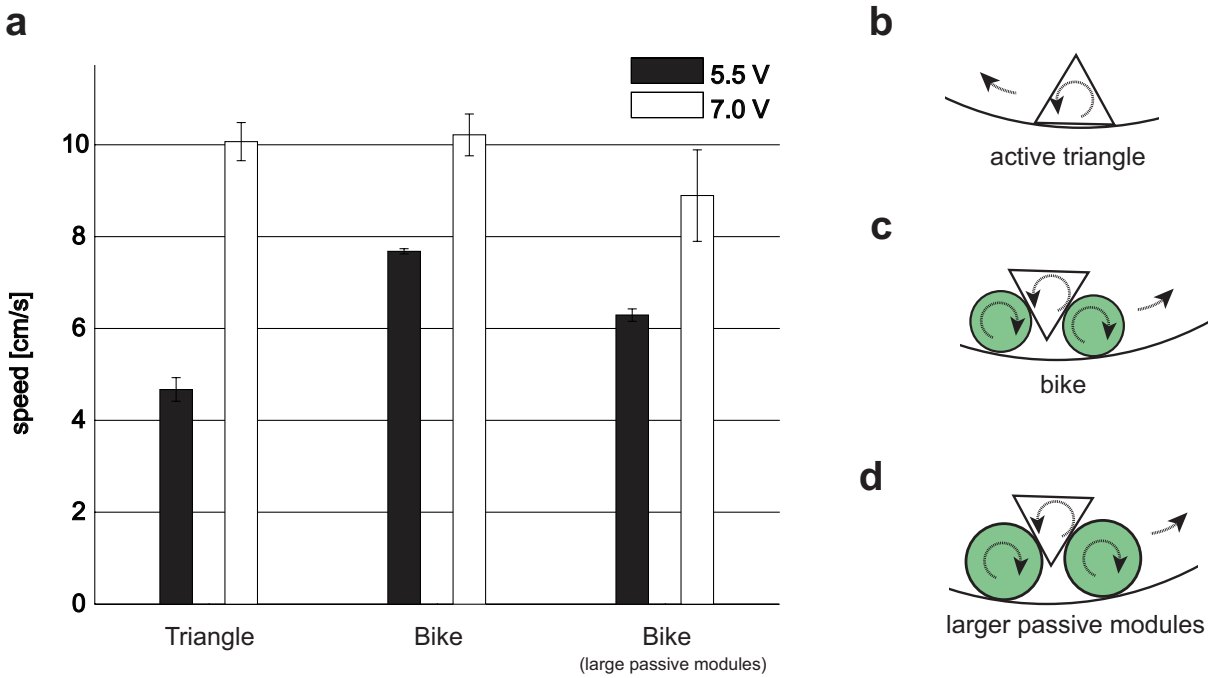

Figure 10: a: Speed of wall following behavior with different configurations of modules, tested under 5.5 V and 7.0 V power supply (n=5). **b-d:** three configurations presented in **a**.

Table 1: Details of modules and experimental setup

vibration motor	FM34F, 13000 rpm (217 Hz), vibration quantity: 17.6 m/s^2, T.P.C
base plate	foam rubber, density: 1.21×10^{-4} g/mm^{-3}, Nicole
permanent magnet	$5 \times 5 \times 5$ mm^3, residual magnetism: 1.3 T, Supermagnete.ch
electrode	Platinum, ϕ 5 mm $\times$ 35 mm
electrolyte water	NaCl, 83.3 g/l
active module	edge length 53.2 mm / surface area: 1225 mm^2 / weight: 3.4 g
passive module	diameter 39.5 mm / surface area: 1225 mm^2 / weight: 1.7 g

Table 2: Details of variables. We intentionally used a different scale of units (e.g. g and kg) in mixed way for intuitive understanding.

$\boldsymbol{g}$	Gravitational acceleration vector	$9.81\,\mathrm{m/s^2}$
m	Mass of the eccentric weight	$0.28\,\mathrm{g}$
M	Mass of the module body	$3.12\,\mathrm{g}$
I	Moment of inertia around the center of mass	$9.9 \cdot 10^{-8}\,\mathrm{m^4}$
L_a	Amplitude of eccentric mass rotation	$5.0\,\mathrm{mm}$
L_l	Height of the pantograph	$45.0\,\mathrm{mm}$
$2L_x$	Side length of the module	$24.4\,\mathrm{mm}$
$2L_z$	Height of the module	$6.2\,\mathrm{mm}$
L_c	Distance between center of mass and center of vibration motor	$4.8\,\mathrm{mm}$
L_d	Distance between the ceiling and water	$45.0\,\mathrm{mm}$
ω:	Angular velocity of vibration motor	$1361\,\mathrm{rad/s}$
k:	Spring constant	$39.2\,\mathrm{N/m}$
c:	Drag coefficient	$1.5 \cdot 10^{-6}\,\mathrm{kg/s}$
μ:	Kinetic friction coefficient	0.47
ρ:	Water density	$1000\,\mathrm{kg/m^3}$